HHS Public Access

Author manuscript

IEEE Trans Radiat Plasma Med Sci. Author manuscript; available in PMC 2024 September 01.

Published in final edited form as:

IEEE Trans Radiat Plasma Med Sci. 2023 September ; 7(7): 692–703. doi:10.1109/trpms.2023.3279455.

Timing Estimation and Limits in TOF-PET Detectors Producing Prompt Photons

Francis Loignon-Houle,
Sherbrooke Molecular Imaging Center of CRCHUS and with the Department of Nuclear Medicine and Radiobiology, Université de Sherbrooke, Sherbrooke, QC J1H 5N4, Canada, currently with Instituto de Instrumentación para Imagen Molecular, Centro Mixto CSIC-Universitat Politècnica de València, 46022 Valencia, Spain

Maxime Toussaint,
Sherbrooke Molecular Imaging Center of CRCHUS and with the Department of Nuclear Medicine and Radiobiology, Université de Sherbrooke, Sherbrooke, QC J1H 5N4, Canada

Émilie Bertrand,
CRCHUS and with the Department of Mathematics, Université de Sherbrooke, Sherbrooke, QC J1H 5N4, Canada

Félix Camirand Lemyre,
CRCHUS and with the Department of Mathematics, Université de Sherbrooke, Sherbrooke, QC J1H 5N4, Canada

Roger Lecomte [Life Senior Member, IEEE]
Sherbrooke Molecular Imaging Center of CRCHUS and with the Department of Nuclear Medicine and Radiobiology, Université de Sherbrooke, Sherbrooke, QC J1H 5N4, Canada, and also with IR&T Inc., Sherbrooke, QC, Canada

Abstract

The production of prompt photons providing high photon time densities is a promising avenue to reach ultrahigh coincidence time resolution (CTR) in time-of-flight PET. Detectors producing prompt photons are receiving high interest experimentally, ignited by past exploratory theoretical studies that have anchored some guiding principles. Here, we aim to consolidate and extend the foundations for the analytical modeling of prompt generating detectors. We extend the current models to a larger range of prompt emission kinetics where more stringent requirements on the prompt photon yield rapidly emerge as a limiting factor. Lower bound and estimator evaluations are investigated with different underlying models, notably by merging or keeping separate the prompt and scintillation photon populations. We further show the potential benefits of knowing the proportion of prompt photons within a detection set to improve the CTR by mitigating the detrimental effect of population (prompt vs scintillation) mixing. Taking into account the fluctuations on the average number of detected prompt photons in the model reveals a limited influence when prompt photons are accompanied by fast scintillation (e.g., LSO:Ce:Ca) but a more significant effect when accompanied by slower scintillation (e.g., BGO). Establishing

This work did not involve human subjects or animals in its research.

performance characteristics and limitations of prompt generating detectors is paramount to gauging and targeting the best possible timing capabilities they can offer.

Keywords

Scintillation detectors; time-of-flight PET; prompt photons; time resolution

I. Introduction

Precise time-of-flight (TOF) information in positron emission tomography (PET) brings an effective noise reduction in the images, the potential for shorter acquisition time or lower injected dose, and the ability to follow a radiotracer for a longer time [1]–[3]. These benefits rely on TOF-PET detectors able to provide excellent coincidence time resolution (CTR) to spatially restrict the position of the annihilation along the coincident line-of-response. Next-generation detectors for ultra-fast TOF in PET might need to diverge from conventional scintillators, especially in order to reach the ambitious goal of 10 ps CTR full width at half maximum (FWHM) [3], [4]. Advances in low-jitter photosensors and readout electronics [5]–[9] must be accompanied by efforts earlier in the detection chain to gain a faster and more efficient signal emission. The time jitter from the readout of scintillators depends on their rise time τ_r, decay time τ_d and number of detected scintillation photons N, which can be used to estimate the initial photon time density and CTR $\propto \sqrt{\tau_r \tau_d / N}$ [10]. Reaching 10 ps CTR with the photon time density of conventional scintillators would be elusive, triggering a demand for a prompter signal emission.

Ultrafast processes are explored by many groups to generate so-called prompt photons having a production time that can be orders of magnitude faster than photons emitted through conventional scintillation processes [11]. A definition of prompt photons might be made with a relation to the single photon time resolution (SPTR) of the photosensor and the light transport jitter, namely that an emission profile shorter than these time smearing effects can be considered as prompt. Herein, we more loosely define that a prompt (or semi-prompt) emission has a decay time <1 ns, the approximate fundamental limit for scintillators dictated by the oscillator strength of a fully allowed radiative transition [12].

Plastic scintillators have decay time constants close to 1 ns, enabling fast timing [13]. They have been joined with denser scintillators in structures allowing energy sharing to provide both fast emission and adequate stopping power [14]–[16].

Another promising detection approach relies on Cherenkov radiation, emitted almost instantaneously and forming a narrow emission peak (analogous to a Dirac delta function) [17]. Cherenkov photons are at the core of numerous detector concepts [18]–[23]. Photodetectors with enhanced detection efficiency matching the Cherenkov emission sparked renewed interest in bismuth germanate (BGO). Recent works have classified BGO signals according to their rising shape, modulated by the fluctuating detection of Cherenkov photons, to segregate the different time resolution categories resulting from the prompt Cherenkov emission and the slow scintillation emission [24]–[27]. The main limitation of Cherenkov-based detectors, however, is the relatively low yield at 511 keV.

Other pre-scintillation phenomena created by the crystal band structure can occur [28]. Hot intraband luminescence is a low yield but fast emission process following the intraband transitions of electrons and holes during their thermalization [29]. Cross-luminescence, originating from transitions between core and valence bands, is another fast process occurring for instance in BaF_2 that has a sub-nanosecond decay time component [30]–[32].

Prompt photons can also be generated by nanostructured materials having faster radiative recombination time compared to bulk scintillators. CdSe nanoplatelets are promising prompt photons generators with higher light yield than Cherenkov or intraband luminescence [33]. These nanoplatelets can be placed in proximity of dense materials that stop the annihilation radiation and enable an energy transfer since they alone have a low stopping power [34]. Perovskite nanoscintillators have also shown fast light emission dynamics [35], [36].

While the production of prompt photons is attracting great interest in experimental research, there is still limited theoretical background dedicated to model prompt generating processes and their influence on CTR. Photon counting statistics in scintillators have extensive theoretical foundations [37]–[39]. The work of Seifert *et al.* [40] was pivotal for the theoretical description of the timing resolution of scintillation detectors in establishing a key formalism based on order statistics and Cramér-Rao lower bound (CRLB), concepts then applied in subsequent works [41]–[43]. This analytical approach, with some simplifications of detector readouts, provides a fast and versatile framework to study a broad range of detector parameters, assess weak links in the detection chain and determine the relative performance or potential suboptimality of real-life timing estimators.

New questions emerge when two distinct photon populations (prompt and scintillation) form the signal. Past investigations based on Monte Carlo or analytical simulations of hypothetical detectors emitting prompt photons motivated their usage for fast timing [17], [44]–[47]. The goal of the present paper is to provide a more robust and extended theoretical basis on the limits in time resolution of detectors that produce both prompt and scintillation photons. We study the effects of the prompt photon emission rate and variability from production to detection. We assess the CRLB on CTR assuming two different photon emission modeling approaches (namely *Joint* and *Split* models, described below), then we compare timing estimators to the lower bounds. We also investigate the performance of *aware* or *blind* estimators which are able or unable to identify the number of prompt photons within a detection set, respectively. This analysis can help shedding light on the limitations and challenges of prompt generating detectors and provide guidelines towards ultimate time resolution in TOF-PET.

II. Methods

In the following, we detail the procedure to assess the lower bound on CTR and timing estimators. These concepts are well established in the literature, but we adapt them for detectors having both a prompt and a scintillation population of photons. We follow similar considerations as in [40]. Namely, we assume detectors able to provide digital timestamps (e.g., multi-channel digital SiPM) and we focus the modeling on the emission and photodetection jitter which are two main mechanisms affecting the CTR. Although

currently in development for future photon counting devices, such digital timestamping still is not fully possible in practice. However, as in [40], this assumption can be useful to study CTR limits and trends with the maximum possible information. We finally extend the model to allow CTR comparison with recent experimental results in the literature for BGO measured with fast analog SiPMs.

A. Signal probability density function

We consider the scintillation emission as a combination of I bi-exponential profiles each with probability $P_{\mathrm{e},i}$

$$p_{\mathrm{em,s}}(t \mid \theta) = \sum_{i}^{I} \frac{P_{\mathrm{e},i}}{\tau_{\mathrm{d},i} - \tau_{\mathrm{r},i}} \left(\mathrm{e}^{-\frac{t-\theta}{\tau_{\mathrm{d},i}}} - \mathrm{e}^{-\frac{t-\theta}{\tau_{\mathrm{r}},i}} \right) \forall t \geq \theta \tag{1}$$

where $\tau_{\mathrm{r},i}$ and $\tau_{\mathrm{d},i}$ are respectively the rise and decay times of the process i and θ is the interaction time of the annihilation photon in the crystal. The emission probability density function (PDF) of the prompt photons $p_{\mathrm{em,p}}(t \mid \theta)$ is assumed as a Dirac delta function at θ or as a fast single bi-exponential profile in the form of Eq. (1). The photosensor time response is defined as a Gaussian profile with mean offset μ_{det} and standard deviation given by the SPTR.

The scintillation and prompt signal PDFs – $p_{\mathrm{s}}(t \mid \theta)$ and $p_{\mathrm{p}}(t \mid \theta)$, respectively—are obtained from the convolution of their emission PDF with the photosensor Gaussian PDF. Photon transport spread was assumed negligible (small detector) to replicate the conditions used in [40] in order to study fundamental limits. Adding this transport in an analytical model complicates the timing error since a bias function needs to be included in the time estimation depending on the interaction position in the detector [48]–[50]. Realistic light transport efficiency (LTE) and photon detection efficiency (PDE) were set at 70% and 60%, respectively. A time step of 0.1 ps was used to model the PDFs.

1) Joint and Split models: In previous works in the literature, the approach to describe the total signal made of two populations of photons was the following. The scintillation and prompt signal PDFs introduced above are merged into a single PDF $p_{\mathrm{ps}}(t \mid \theta)$ using a weighting from the relative number of photons of each population

$$p_{\mathrm{ps}}(t \mid \theta) = \frac{M}{M+N} \cdot p_{\mathrm{p}}(t \mid \theta) + \frac{N}{M+N} \cdot p_{\mathrm{s}}(t \mid \theta) \tag{2}$$

where M and N are the expected number of detected prompt photons and scintillation photons, respectively. Simulations using this merged PDF therefore requires drawing $M + N$ samples to obtain photon detection timestamps. This model will be referred to as the *Joint* model.

A new model proposed here keeps the prompt $p_{\mathrm{p}}(t \mid \theta)$ and scintillation $p_{\mathrm{s}}(t \mid \theta)$ PDFs separate. The PDFs underlying the two models are shown at the top of Fig. 1. Simulations using the second model requires drawing M samples from the prompt PDF and N samples

from the scintillation PDF. The motivation for introducing this model, which will be referred to as the Split model, is mainly twofold.

First, it correctly affects the number of samples to its physical origin by drawing photons from their source PDF, i.e., M photons from $p_{\mathrm{p}}(t \mid \theta)$ and N photons from $p_{\mathrm{s}}(t \mid \theta)$. Extracting $M + N$ timestamps from the Joint model PDF $p_{\mathrm{ps}}(t \mid \theta)$ could statistically give events having more than M timestamps from the prompt time range, thus yielding more prompt photons than physically allowed. Conversely, a Joint model with a PDF built from the expected average M and N contains fixed information, which would, for example, overestimates the information available for events having zero detected prompt photons. Second, the *Split* model enables the inclusion of potential photon discrimination. It is thus possible to adopt dedicated estimation methods able to categorize events made from various numbers of detected prompt photons.

B. Fisher information and Cramér-Rao lower bound

Series of timestamps of (not necessarily ordered) detected prompt photons $T_{\mathrm{p}} = \{t_{\mathrm{p}1}, \ldots, t_{\mathrm{p}M}\}$ and scintillation photons $T_{\mathrm{s}} = \{t_{\mathrm{s}1}, \ldots, t_{\mathrm{s}N}\}$ form an ensemble of all recorded photons $T = \{T_{\mathrm{p}}, T_{\mathrm{s}}\}$, where we assume that T_{p} and T_{s} are independent from each other and are respectively independent and identically distributed (iid). There could also be dependence between the prompt and scintillation populations of photons, an aspect discussed in Sec. IV-F. For the *Split* model introduced in Sec. II-A, which keeps separate the prompt and scintillation PDFs, the log-likelihood function is

$$l(\theta \mid T) = \sum_{i=1}^{M} \ln\, p_{\mathrm{p}}(t_{\mathrm{p}i} \mid \theta) + \sum_{j=1}^{N} \ln\, p_{\mathrm{s}}\left(t_{\mathrm{s}j} \mid \theta\right). \tag{3}$$

We define $l_{\mathrm{p}}(\theta \mid t_{\mathrm{p}})$ as the log-likelihood function for one prompt photon and $l_{\mathrm{s}}(\theta \mid t_{\mathrm{s}})$ for one scintillation photon. The Fisher information is then

$$\mathcal{I}(\theta) = E_{\theta}\left(-\frac{\partial^2}{\partial\theta^2}\left(\sum_{i=1}^{M} l_{\mathrm{p}}(\theta \mid t_{\mathrm{p}i}) + \sum_{j=1}^{N} l_{\mathrm{s}}\left(\theta \mid t_{\mathrm{s}j}\right)\right)\right) \tag{4}$$

$$\overset{iid}{=} M \cdot \mathcal{I}_{\mathrm{p}}(\theta) + N \cdot \mathcal{I}_{\mathrm{s}}(\theta) \tag{5}$$

where $\mathcal{I}_{\mathrm{p}}(\theta)$ and $\mathcal{I}_{\mathrm{s}}(\theta)$ are the Fisher information for one prompt photon and one scintillation photon, respectively. The standard form of the Fisher information, given by

$$\mathcal{I}(\theta) = \int_{-\infty}^{\infty} \left(\frac{\partial}{\partial\theta} \ln\, p(t \mid \theta)\right)^2 p(t \mid \theta)\, \mathrm{d}t, \tag{6}$$

can be used to evaluate $\mathcal{I}_{\mathrm{p}}(\theta)$ and $\mathcal{I}_{\mathrm{s}}(\theta)$ by using $p_{\mathrm{p}}(t \mid \theta)$ or $p_{\mathrm{s}}(t \mid \theta)$. With the *Joint* model where a single PDF describes the signal, a single Fisher information $\mathcal{I}_{\mathrm{ps}}(\theta)$ is calculated using the merged PDF $p_{\mathrm{ps}}(t \mid \theta)$ (Eq. (2)).

The Cramér-Rao bound establishes a lower bound on the variance of any unbiased estimator $\hat{\theta}$ of θ and is equal to the inverse of the Fisher information. The CRLB can be computed using the *Split* and *Joint* models as

$$\mathrm{CRLB}_{Split} = \frac{1}{M \cdot \mathcal{J}_{\mathrm{p}}(\theta) + N \cdot \mathcal{J}_{\mathrm{s}}(\theta)} \tag{7}$$

$$\mathrm{CRLB}_{Joint} = \frac{1}{(M + N) \cdot \mathcal{J}_{\mathrm{ps}}(\theta)} \tag{8}$$

giving the minimal variance on $\hat{\theta}$ for a single detector. The lower bound on CTR for detectors in coincidence, converted to FWHM, is normally reported as $\mathrm{CTR} = 2.355 \times \sqrt{\mathrm{CRLB}^{(\mathrm{A})} + \mathrm{CRLB}^{(\mathrm{B})}}$ for detectors A and B. This conversion might be inadequate because of possible non-Gaussian timing distributions. However, throughout this paper, we report CTR values obtained from the standard deviation of the raw coincidence data (σ_{coinc}) multiplied by the 2.355 factor. This allows representing the true timing variance and easier interpretation in relation to conventional FWHM values of Gaussian coincidence timing.

The modeling distinction between the *Split* and *Joint* models is illustrated in Fig. 1. The order statistics PDFs differ between the two models and a sampling of the photons from these PDFs can give different outcomes. The *Split* model can correctly assign the number of samples to its source and lower bounds assessed with this model (Eq. (7)) therefore result from an estimation inherently *aware* of the photon nature, contrary to the *Joint* model where photon identity is ignored.

C. Adding fluctuations to the photon yields

The fluctuations on the number of detected photons are important to consider to correctly describe and model the CTR. The impact of coincidences with different numbers of prompt photons on CTR has already been shown prominent in BGO [24]. Fluctuations of the yield of (prompt) photons can be readily included in Monte Carlo simulations, for instance on the Cherenkov yield related to the photoelectron stochastic path [13], [51]. For analytical modeling, the authors of [40] have included the probability $\mathbb{P}(N)$ of detecting N scintillation photons (derived from the energy resolution of the scintillator) in CRLB calculations, i.e., $\mathrm{Var}(\hat{\theta}) \geq \sum_N \mathbb{P}(N)/(N \cdot \mathcal{J}_{\mathrm{s}}(\theta))$. They found a minor impact of this variability since N is typically large. The lower yield of prompt photons could make their fluctuations more significant. The need to account for the prompt yield variability in analytical modeling was pointed out in [52].

We thus consider a detector where the number of detected prompt photons is subjected to fluctuations described by probability $\mathbb{P}(M)$. Rewriting the CRLB of the Split model (Eq. (7)) with fluctuations for both photon populations gives

$$\mathrm{CRLB}_{Split} = \sum_M \sum_N \frac{\mathbb{P}(M)\mathbb{P}(N)}{M \cdot \mathcal{J}_{\mathrm{p}}(\theta) + N \cdot \mathcal{J}_{\mathrm{s}}(\theta)} \tag{9}$$

assuming independence between the two populations. Because of the minor impact of fluctuations of the larger N, we kept it fixed in the present work to focus on the effect of $\mathbb{P}(M)$ on CTR. Analytical results obtained with the *Joint* model in this work and in the literature assumed no explicit fluctuations. The number of photons modifies the *Joint* model PDF (Eq. (2)) and would require calculating the Fisher information for each possible M and N. Nonetheless, an indirect but interesting feature of the *Joint* model is a possible intrinsic photon yield variability. Indeed, the sampling of the merged PDF with $M + N$ photons can induce an event-by-event variability on the number of timestamps extracted from the prompt time range. Still, it was not demonstrated whether this is an accurate modeling of prompt variability compared to a disjoint sampling of two PDFs with physics-based assumptions about fluctuations on the production and detection of the samples. We thus assess CTR values obtained with the *Split* model assuming fluctuations and compare them with the *Joint* model.

D. Timing estimators

Timing estimators in scintillation detectors have been proposed in the past with their performance compared to the CRLB [40], [42], [53]. An analysis combining both CRLB calculations and simulations makes it possible to evaluate the potential optimal performance of a detector as well as the requirements for estimators to reach this potential. A set of ordered timestamps $T = \{t_1, t_2, \ldots\}$ is obtained from the detection of photons. A timing estimator based on a simple average was computed using these timestamps. We define q as the order of a timestamp in the set and Q as the maximum utilized order by an estimator, so $q = 1, \ldots, Q$ and $Q = 1, \ldots, 50$ (we fix $Q \leq 50$ in this work). The timing estimation is done with

$$\hat{\theta}(Q) = \frac{1}{Q} \sum_{q=1}^{Q} t_q \tag{10}$$

with t_q being the q^{th} photon of T. A Gauss-Markov timing estimator [53] was also tested using the covariance matrix of all primary triggers with orders below Q. We now describe the creation of T for the *Joint* and *Split* models.

1) Joint model estimators: With the Joint model, $M + N$ samples were drawn from the merged PDF of Eq. (2), ordered in time, and the first 50 were kept to create a timestamp dataset defined as $T^{(Joint)}$. This process was repeated 20000 times for two detectors. For each event in a coincidence between the two detectors, $T^{(Joint)}$ was inserted in Eq. (10) and the time difference between the estimate in each detector was evaluated for each estimator order Q. The CTR was computed taking the standard deviation of the time difference distribution multiplied by 2.355. The best CTR among the estimator order was finally retained. This whole process, including the creation of the merged PDF, was then repeated for each M of interest.

2) Split model estimators: With the *Split* model, the prompt and scintillation photons were drawn independently from their respective PDFs. In contrast to the *Joint* model, the PDFs only need to be computed once as they do not change depending on M and N. The

process starts by fixing an average number of generated prompt photons M_{gen}. A range of probable generated prompt photons is then created assuming a Poisson distribution with parameter M_{gen}. With the light transfer efficiency and photon detection efficiency, the average number of detected prompt photons is given by LTE $\times$ PDE $\times M_{\text{gen}}$. A binomial distribution with probability LTE $\times$ PDE is used to create a range of probable detected prompt photons. The probability $\mathbb{P}(M)$ of detecting M prompt photons is thus obtained from the combination of these two processes, illustrated in Fig. 2. The model allows any choice of distribution to include the fluctuations, i.e., not limited to Poisson and binomial processes.

A dataset of $\Phi = 50\,000$ event pairs was partitioned using $\mathbb{P}(M)$. Thus, the frequency of an event having m detected prompt photons in the dataset is $\Phi \times \mathbb{P}(M = m)$. For each event and detector, a group of the first 50 time-ordered photons was made, i.e., $T^{(Split)}_{\text{grouped}} = \text{sort}\{T_{\text{p}}, T_{\text{s}}\}$ with T_{p} obtained by sampling the prompt PDF m times following the partitioning. Timing estimations were done for all events using Eq. (10) and coincidence times between two detectors were calculated. Shuffled events distributed along $\mathbb{P}(M)$ generate coincidences formed from various M combinations, and the CTR is thus directly obtained from the variance (converted to FWHM) of the coincidence distribution. This estimation using a *blind* mix of the prompt and scintillation populations therefore does not retain any information about the nature (prompt vs scintillation) of the photons.

Another estimator, developed by assuming the ability to identify the photon nature, consisted of using an estimation *aware* of the number of detected prompt photons in each event, thus allowing an estimation adapted for each possible M. To do this, we kept separate each dataset of a given M (1000 events for each M) and the estimator order having the lowest variance is retained

$$\widetilde{Q}_M = \arg\min_{Q} \left\{ \text{Var}\left(\hat{\theta}(Q) \mid M \right) \right\}. \tag{11}$$

Timing estimators might be biased depending on the difference in the number of detected prompt photons in coincident detectors, thus for each M, the mean time offset of the estimator was subtracted from the timing estimate

$$\hat{\theta}^{(Split)}_{aware} = \hat{\theta}(\widetilde{Q}_M) - \text{Mean}\left(\hat{\theta}(\widetilde{Q}_M) \right). \tag{12}$$

This unbiasing is analogous to different depths of interaction (DOI) in ultrafast detectors inducing a time bias which can then be corrected from a DOI estimation [50]. The CTR is then obtained by a weighted sum of the variance for each possible combination of detected M, defined by $\mathbb{P}(M)$ in both detectors, taking the square root and multiplying by 2.355.

From now on, timing estimation using a timestamp set without information on the number of detected prompt photons will be referred to as a *blind* estimation as opposed to an *aware* estimation when the information is assumed available, as illustrated at the bottom of Fig. 2. For the Dirac delta prompt emission, the CTR was assessed as a function of the mean

number of detected prompt photons from 0 to 25. For the fast bi-exponential semi-prompt emission (rise and decay times of 10 ps and 500 ps, respectively), the CTR was assessed as a function of the photon time density (mean number of detected prompt photons divided by the product of the rise time and the decay time) from 0.001 to 0.1 photon/ps^2. The choice of these semi-prompt emission parameters was inspired by existing materials having fast emission with decay components in the range of a few hundreds of picoseconds [34], [54]. The SPTR was chosen to either study the CTR with currently achievable SPTR performance (30 ps rms) or to study potential future performance (10 ps rms) while looking at the CTR improvement as a function of the number of prompt photons or prompt photon time density.

E. Comparison with CTR in the literature for BGO

We compared the CTR obtained with the simulation model to the experimentally measured CTR of BGO found in [25]. We used experimentally measured parameters (in [13]) of a 2×2×3 mm^3 BGO (τ_r = 8 ps, τ_d = 46/365 ns (8%/92%)) and a FBK NUV-HD SiPM (SPTR=30 ps rms) to compute the emission and detection PDFs. A dedicated photon transport spread (PTS) PDF for the Cherenkov and scintillation transport was obtained with GATE v9.0 [55] using the LUTDavis reflectance tables assuming polished crystal wrapped in Teflon [56]. The LTE for the scintillation and Cherenkov photons was set to 64% [13] and 30% [57], respectively, while the PDE was set to 47% and 39% [13]. Timestamps were extracted from the *Split* model PDFs and fluctuations on the prompt yield (17 generated Cherenkov photons on average with 30% amplitude Gaussian fluctuations [13]) were included as detailed in Sec. II-D. The dataset was thus formed with events distributed following the DOI and Cherenkov yield probabilities. Optical crosstalk in the SiPM, which has been shown to be less important for the CTR compared to other factors [13], [58], was not included in this simulation. A single photon avalanche diode (SPAD) signal was modeled using a measured average of many single dark count events aligned on their maximum slew rate in a high-frequency readout setup, the same as the one used in [13]. A signal pile-up of SPAD signals starting at the simulated timestamps was done to emulate an analog SiPM signal. We then extracted the crossing times at a leading edge threshold of 10mV, performed coincidences and evaluated the CTR FWHM and FWTM to compare with the values in [25].

III. Results

A. Prompt emission rate and fluctuations

The CRLB on CTR of the *Split* model as a function of the prompt emission decay time for various prompt yields, with or without fluctuations, is shown in Fig. 3. We remind that using the CRLB formalism with the *Split* model gives CTR values resulting from an *aware* estimation (see Sec. II-B). The scintillation component was defined either with slow decay time and low light yield (e.g., BGO-like) or fast decay time and high light yield (e.g., LSO:Ce:Ca-like). In all cases, the CTR rapidly degrades when the prompt emission decay time increases. Assuming a prompt emission as a pure delta peak is a special case enabling ultrahigh time resolution, but CTR predictions should consider prompt emission kinetics. A higher prompt photon yield however relaxes the need of having a faster prompt emission. The added fluctuations have a stronger impact in the detector with slower scintillation when the average number of prompt photons is low. When a detection set contains events

with zero detected prompt photon, the scintillation can become highly critical for CTR as also seen experimentally with BGO [24]. Increasing the average prompt yield mitigates the negative effect of fluctuations. In the detector with faster scintillation, the prompt photon fluctuations have a negligible impact on the CTR since the scintillation itself provides high photon time density. CTR predictions considering a fixed average prompt yield would therefore appear reliable when fast scintillation is available.

B. Lower bounds on CTR and estimators

The CRLB on CTR and the CTR of *blind* and *aware* estimators (average estimation, see Sec. II-D) using the *Joint* and *Split* models are shown in Fig. 4a for a Dirac delta prompt emission. The cases of prompt photons accompanied either by a slow or a fast scintillation population are shown. Fast scintillation, unlike slow scintillation, can prevent the strong CTR degradation at lower prompt yield, as previously observed in Fig. 3. The CTR of the Gauss-Markov estimator was also evaluated and gave similar trends. With slow scintillation (top plot), the CRLB-*Joint* appears to predict overoptimistic CTR values at the lower prompt yield, which almost match the CRLB-*Split* predictions when neglecting fluctuations. This is suggesting that the impact of fluctuations on the CRLB are not described adequately by the *Joint* model for this detector type. With fast scintillation (bottom plot), the *aware* estimator matches the CRLB-*Split*, showing its advantage against the *blind* estimator. The *Joint* model appears as a good surrogate for a *blind* estimation since *Split-blind* and *Joint* estimators yield almost identical performance. Sampling a single merged PDF with the total number of photons seems analogous as sampling independently the PDFs with fluctuations and merging blindly the samples.

The same curves are shown in Fig. 4b, this time for a semi-prompt emission. The CTR is plotted as a function of the photon time density and was computed by varying the number of prompt photons between 5 and 500, giving photon time densities spanning from 0.001 to 0.1 photon/ps^2 (10 ps rise time and 500 ps decay time). The same photon density range calculated with other values of decay time and prompt yield gave the same CTR, as long as the decay time is sufficiently high (estimated at $\gtrsim$ 100 ps for a 10 ps rise time). The *Split-blind* and *Joint* estimators yield similar CTR as also seen in Fig. 4a and a new similarity is observed for the CRLB of both models. As the CRLB-*Split* is constructed from an *aware* estimation and assuming the CRLB-*Joint* represents a *blind* estimation, there is therefore no apparent distinction between being *blind* or *aware* in terms of lower bounds on CTR for a semi-prompt emission. The tested estimators are however still not fully efficient since there is still a gap between them and the CRLB curves. The CRLB might also be too optimistic, an aspect discussed in Sec. IV-E. With the fast scintillation, the aware estimator gives only marginal CTR gain compared to the *blind* estimator, whereas all estimators are overlapping for the detector with slow scintillation.

The required characteristics to reach certain CTR values differ between a Dirac delta peak and bi-exponential emission profiles. Targeting the goal of 10 ps CTR, we see that $\gtrsim$ 10 mean detected prompt photons are required with an aware estimation (CRLB-*Split* in Fig. 4a with SPTR of 10 ps rms). Nearly twice as many prompt photons are required for a *blind* estimation in the detector with fast scintillation (CRLB-*Joint*). Photon time densities

above 0.1 photon/ps^2 would be necessary to reach 10 ps CTR for both models with a bi-exponential emission profile as seen in Fig. 4b, corresponding, for example, to 500 detected semi-prompt photons with 10 ps rise time and 500 ps decay time. This analysis is applicable for lower bounds on CTR, thus worse SPTR, PTS and noise would set even more stringent requirements.

C. Overlap of the prompt and scintillation signals

The overlap between the prompt and scintillation PDFs can help explain the CTR difference between *blind* and *aware* estimations. The CTR gain of being aware as a function of the overlap is shown in Fig. 5. Lower bounds assessed with the *Split* model result from an *aware* estimation, whereas the *Joint* model adequately represents a *blind* estimation with fast accompanying scintillation (Fig. 4). The gain is thus calculated from the ratio between the CRLB of the *Joint* and *Split* models. Varying the overlap was done by offsetting in time the scintillation PDF. The same procedure was also done by increasing the rise time of the scintillation to vary the overlap, showing similar conclusions. At small overlap where the photon populations are well separated, identifying the photons provides no CTR gain since no photon mixing occurs. The integration domain to compute the Fisher information is disjoint for the non-null part of the two PDFs, so merging the PDFs and computing the Fisher information provides the same result as summing the Fisher information computed separately for the two PDFs. For growing overlap, population mixing starts occurring and photon identification becomes desirable to provide an estimation optimized according to the fluctuating number of detected prompt photons. The gain eventually decreases for large overlap where the populations are fully mixed. The overlapping first order statistics of the two populations have limited relative time bias, so adapting an estimation with bias correction (see Eq. (12)) gives marginal gain. Although this overlap is not introduced as a predictive CTR gain metric for any detector types, it can still provide an indication of when being *aware* of photon nature is favorable for CTR. Furthermore, even when there is no overlap between the prompt and scintillation PDFs, the timing estimation for an event containing zero detected prompt photon can be improved with an *aware* estimator. For this specific case, the time shift could thus be corrected to improve the CTR.

D. Comparison with CTR in the literature for BGO

BGO crystals emit both scintillation and prompt (Cherenkov) photons. The *Split* model was used to extract simulated timestamps from which a CTR was evaluated, assuming an analog readout (single photon response function for each detected photon, pulse pile-up and leading edge discrimination, see Sec. II-E) of a 2×2×3 mm^3 BGO crystal with a FBK NUV-HD SiPM. A comparison with experimental measurements obtained from [25] is shown in Fig. 6. The simulated CTR is in good agreement with the measured CTR, both for the FWHM (188 ps vs. 198 ps) and FWTM (455 ps vs. 465 ps). The coincidence time distributions were both fitted with a double-Gaussian fit including a narrower component mostly driven by the faster Cherenkov photons and a broader component driven by the slow scintillation light, the latter giving the known tails of BGO timing distributions. For this simulation, ~15% of the events had no detected Cherenkov photon in each detector which therefore contributed to this second broader fit component. The *Split* model was used for this simulation, but a similar performance might be expected with the *Joint* model since it was observed that a

blind estimator with the *Split* model is equivalent to the *Joint* model estimator (Fig. 4a). However, since the light transport in finite crystal length was modeled here, the *Split* model was chosen due to its ability to model the PTS separately for both photon populations.

IV. Discussion

A. Prompt emission kinetics

Considering a prompt emission as a Dirac delta peak leads to outstanding CTR values, which partly motivated the usage of prompt photons to reach 10 ps CTR, although this nearly instantaneous emission might only be an approximation for Cherenkov photons. The first CRLB results (using a model with merged PDFs) with a non-Dirac delta prompt emission were recently reported for a meta-scintillator (LSO:Ce:Ca host and CdSe nanoplatelets with semi-prompt kinetics) [3]. Compared to a pure prompt emission, these results indicated a higher required photon yield necessary to reach 10 ps CTR. Extending the results of [3], Fig. 3 shows the swift CTR degradation with increasing (semi-)prompt decay time. It is however expected that the light yield of a semi-prompt emission might be much higher than a pure prompt emission [33], possibly leading to similar photon time densities.

B. Prompt/scintillation signals overlap

An excellent discussion on fast timing with prompt photons is found in [17] which highlighted that high bandwidth amplifiers and fast SiPM single cell rise time are needed to harvest the best timing from prompt photons. Electronic noise limits the use of very low thresholds with analog leading edge discrimination. High bandwidth electronic was recently developed [5], [6], enabling state-of-the-art CTR for many scintillators [13]. Going from analog to digital—recording individual timestamps with a digital SiPM or photon-to-digital converter [8]—can also be advantageous. Indeed, this would avoid the bandwidth and electronic noise limitations, and thus allow efficient detection of the faint signals from prompt photons with enhanced CTR, notably for low SPTR values [13]. The authors of [17] also pointed out that scintillation with slower rise time and lower yield might enable natural discrimination of a prompt population detected earlier than the scintillation. This would allow prompt photons to determine the timing without interference from the scintillation, analogous to the *aware* estimation introduced in this paper. The CTR difference resulting from the type of estimation (*aware* vs. *blind*) was found dependent on the overlap between the prompt and scintillation PDFs (Fig. 5).

C. Merging of the PDFs and estimators

In crystals emitting scintillation and prompt photons such as LuAG:Pr, LuYAP:Ce and BGO, their emission measured with a time correlated single photon counting setup appears as a single profile having an intensity burst at its onset [17]. Fitting this profile can be done with a function summing a prompt part and a scintillation part with relative intensity adapted to the height of the prompt burst. Whereas a single merged PDF (*Joint* model) is perfectly suitable for fitting, evaluating timing estimators and lower bounds with this *Joint* model might miss the underlying independence of the emission mechanisms. Order statistics extracted from distinct PDFs or from a single merged PDF are not always equivalent (Fig. 1). For example, the CRLB of the *Split* and *Joint* models can be different (Fig. 4a). It was

however seen that sampling the single merged PDF with the total number of photons seemed equivalent as sampling independently the PDFs with fluctuations and merging blindly the samples, i.e., the *Joint* and *Split-blind* estimators had similar CTR (Fig. 4a and 4b). Also, modeling semi-prompt photons with both the *Joint* and *Split* models yielded similar results (Fig. 4b). Therefore, even though a *Joint* model was used to simulate the scintillation processes (Eq. (1)), it is expected that using a *Split* model would give negligible difference since the scintillation components have higher yields and decay times. A notable feature of the *Split* model is the ability to use functions and parameters dedicated to each photon regime, e.g., light collection efficiency and PDF, and SiPM PDE, as done in Fig. 6.

The Gauss-Markov estimator yielded similar CTR as the average estimator in the present study, but can however provide better CTR convergence and stability as a function of the estimator order depth [48], [53]. The *aware* estimation for the detector with fast scintillation was efficient (close to the CRLB), but deviates from the CRLB at low photon yield with slow scintillation (Fig. 4). This apparent inefficiency might stem from the multimodal nature of the time distribution of prompt and slower scintillation photons, limiting an optimal timing estimation. It might also come from a lack of tightness of the CRLB at low photon sampling [59], [60]. This is further analyzed in Sec. IV-E. Noise sources such as optical crosstalk and dark counts in the SiPM can reduce the accuracy of timing estimators and were not included in the present study aimed at assessing fundamental limits as in [40]. Lower bounds are still important to report for gauging the full potential of prompt generating detectors without confining the study to a specific readout noise level. A next step would also be to fully consider photon transport in the models. In this case, tackling the problem of DOI estimation adapted for prompt generating detectors with non-negligible length is important, driven by the necessity of preserving sensitivity in PET imaging.

D. Photon discrimination

Discrimination of the photon regime might be complex to achieve. Prompt photons could possibly be distinguished from scintillation photons using different techniques. The spectral profile of different photon production processes can vary, so wavelength evaluation might provide some discrimination power, although wavelength filters can deteriorate the time resolution [61]. Statistical assumptions on the arrival time distribution might provide insights on photon discrimination by using the order statistics of prompt and scintillation photons to infer the source of the n^{th} detected photon. Analysis of the signal shape already provides some statistical insights into events containing different numbers of prompt photons. Indeed, classification of events depending on the signal rise time and time resolution driven by the number of detected Cherenkov photons was successfully achieved in BGO [24], [27]. Structured assemblies separating the prompt and scintillation emitters with a spatially-adapted readout could also be suitable to yield some photon discrimination capabilities. For instance, event-by-event measurement of the shared energy between a prompt emitting material in metascintillators can also provide an estimation of the relative amounts of prompt and scintillation photons [15], [16]. The time resolution of these analog detectors can then be improved with a time-walk correction, which can be considered as an *aware* unbiasing estimation. Choosing an image reconstruction kernel with detectors generating various numbers of prompt photons is therefore an important aspect, recently explored in

[26]. The *Split* model, compared to the *Joint* model, is advantageous in this regard, because it enables event categorization from the underlying fluctuations coupled to the ability of creating dedicated estimators for the *blind* or *aware* situation.

At very high time resolution, a gain of a few picoseconds can be considered substantial, so the complexity of the readout needed to achieve photon identification must be weighted against the potential gain. For instance, there is only a small gap between the CTR of *blind* estimators and *Split* (*aware*) CRLB for semi-prompt emission with fast scintillation (Fig 4b). The *aware* estimator, built by only discriminating the number of detected prompt photons (no prompt/scintillation ordering identification), reached the CRLB for the Dirac delta prompt emission with fast scintillation (Fig 4a). Estimators *aware* to the photon ordering might be needed for higher gain in the case of a detector with slow scintillation. We also showed that the gain arising from photon identification can depend on the overlap between the signals (Fig. 5).

E. Limitations of the CRLB

A limitation of the CRLB can arise from rapid time-intensity evolution of a faint signal formed with prompt photons, leading to possible pathological numerical behavior in Eq. (6) with CRLB possibly approaching zero. This was pointed out in [52], which also referred to other works in which a lower bound on the mean-squared error (MSE) of TOF estimators was proposed [59], [60]:

$$\mathrm{MSELB} = \Lambda^{-2}\left(\sum_i \frac{\alpha_i}{\tau_i}\right)^{-2} \tag{13}$$

where τ_i is the i^{th} decay constant with weight α_i and Λ is the light output. This bound was found tighter, showing less optimistic CTR than the CRLB for scintillators with moderate light yield and long decay like BGO. However, the bound does not account for the timing degradation due to light collection and photodetector jitter. It might therefore, for instance, miss the increasing importance of this jitter on CTR at good SPTR values, especially for digital detection approaches [13].

As a complementary analysis to discuss CRLB limitations in the context of prompt photons, we report here the CTR obtained with this lower bound with conversion to FWHM in coincidence, i.e., $2.355 \times \sqrt{2} \times \sqrt{\mathrm{MSELB}}$. We consider the standard scintillation of BGO (46/365 ns (8%/92%) decay times, 10 700 phMeV^{-1} with total detection efficiency of 0.42) accompanied by a population of semi-prompt photons with 10 ps rise time, 500 ps decay time and detected yield varying between 2 and 500 photons. Inserting these three decay components in Eq. (13), with weighting adapted to the amount of prompt photons, yields the CTR displayed in Fig. 7 compared to the average *blind* estimator and the CRLB of the *Split* model. This reprises the CRLB and estimator in the top of Fig. 4b which were both similar to the *Joint* model curves.

The MSE bound provides a better description of the CTR trend obtained with the average estimator at lower prompt photon time density. This is similar to what was found in

[59] for smaller values of Λ where the CRLB diverges by predicting lower timing error compared to the MSE bound and estimators. Nonetheless, the purpose of prompt photons in next-generation detectors is to reach CTR towards tens of picoseconds where the CRLB seems more adequate since the estimator almost exactly matches it.

For fast, high-yield scintillation accompanying the prompt populations, the CTR of timing estimators (Fig. 4) can approach the CRLB. These estimators do not rely on the Fisher information calculation and they are therefore immune to the pathological behavior discussed above. This suggests that the CRLB can be reliable in that case. Other bounds [62] could also be investigated in a future study.

Another potential numerical limitation of the CRLB is related to the choice of time discretization in the modeling. We computed the CRLB for various parameters of the prompt emission (rise time, decay time and yield) using different time steps from 0.1 ps to 20 ps to create the signal PDFs. Time steps in the 0.1–5 ps range gave no CRLB difference. In the 5–10 ps range, the CRLB predicted better CTR by <10%. At 20 ps time step, larger differences occurred, going up to 25% better CRLB compared to a 0.1 ps time step. For all prompt emission parameters, the biggest discrepancies between larger time steps and 0.1 ps time step were observed for weaker signals. A coarser sampling rate might thus deliver overoptimistic CRLB. The CRLB is also known to be overly optimistic in some specific cases, for example when the PDF is a single decaying exponential function, predicting a $1/N$ improvement in standard deviation, N being the number of detected photons. This $1/N$ improvement was also found in initial works on photon counting statistics [37]. The now better known $1/\sqrt{N}$ improvement of CTR can be retrieved when the scintillation emission is modeled by also including the rise time and when the emission PDF is convolved with the transport and photodetection PDFs.

F. Prompt generating detector concepts

The benefits of an hypothetical high-yield prompt emitter were extensively investigated in recent years to define criteria for reaching ultrafast timing [10], [17], [44]–[47], [63]. Similar investigations were performed to define the needed, although still not achieved, PDE and SPTR of SiPMs to reach CTR values [17], [18], [47], [50], [64] with progresses achieved over the past few years [13], [65], [66]. Improved methods or materials able to generate higher prompt yields are needed to achieve the CTR gains observed in Fig. 4. Nanostructuration enables changes of properties in materials, which has made it possible to promote novel phenomena being exploited in many fields [67], but this has remained quite unexplored in the field of radiation detectors until now. One novel concept proposed in [14] is through energy sharing—which depends on the primary electron path [68]—between bulk dense scintillators and prompt-emitting nanocrystals. Another concept is through a photonic crystal approach where the nanostructuration scale enables coherent effects, boosting the intrinsic yield of standard bulk scintillators from the Purcell effect [69]–[71]. Also, lowering the Cherenkov production threshold is possible in nanostructured or two-dimensional materials [72]. Applying this feature in the context of a primary electron produced upon the interaction of annihilation photons might enable the production of Cherenkov photons below the conventionally required high-energy threshold.

Finally, detectors based on the detection of two populations of photons are still in active investigation and new concepts could emerge. A case-dependent modeling might be needed as two fundamental conditions arise in prompt generating detector concepts: a possible coupling scheme of the prompt and scintillation photons (energy sharing of the annihilation photon) and a possible identification of the emission regime of individual photons. The combination of these situations therefore leads to four possible general concepts (uncoupled/coupled and *aware*/*blind*). Here, we have focused on the uncoupled situation for which the amount of prompt photons is independent of the scintillation yield, but Eq. (9) can be rewritten by incorporating a link between the two populations. In a coupled case, augmenting the prompt yield for an event reduces the scintillation yield because of the annihilation photon energy sharing. CRLB calculations were recently done for the situation where the 511keV energy is shared stochastically event-by-event between two materials [15]. Ultimately, timing estimators and lower bounds could therefore be adapted for these various concepts based on the (in)dependence of the signal sources and their potential identification.

V. Conclusion

A model of the time resolution of detectors producing both scintillation and prompt photons was proposed. Building on previous work in the literature, we included aspects such as population-dependent statistical sampling, emission rate and prompt yield fluctuations both for timing estimators and theoretical lower bounds. More stringent requirements for fast timing emerge on the photon yield for semi-prompt (fast bi-exponential) emission compared to the commonly assumed instantaneous emission. The influence of including prompt photon fluctuations is weak when accompanied by fast scintillation (e.g., LSO:Ce:Ca) but becomes more significant when accompanied by slower scintillation (e.g., BGO). The modeling of double-population statistics was refined by assuming estimators *blind* or *aware* to photon nature (prompt vs scintillation), in the latter case to mitigate the detrimental effect of population mixing on timing when the signals overlap. *Aware* estimators can also help to filter events containing slow-emission scintillation photons causing high-variance, non-Gaussian timestamp distribution. Such filtering, already reported experimentally in the literature, was recreated with the proposed modeling, which at the same time provided indications on timing limits. The more elaborate theoretical description of prompt generating detectors strengthens the assessment of their high potential for ultrafast timing.

Acknowledgments

The authors would like to express their gratitude to Nicolaus Kratochwil and Carlotta Trigila for their input on the BGO experimental measurements and simulations, respectively. The Sherbrooke Molecular Imaging Center is a member of the FRQS-funded Research Center of CHUS (CRCHUS). Roger Lecomte is a co-founder and Chief Scientific Officer of IR&T Inc. All authors declare that they have no known conflicts of interest in terms of competing financial interests or personal relationships that could have an influence or are relevant to the work reported in this paper.

This work was supported by grants from the Natural Sciences and Engineering Research Council of Canada, Mitacs and the MEDTEQ Consortium of the *Ministère de l'Économie, de l'Innovation et de l'Énergie* of the Government of Québec, and U01 EB027003 from NIH.

References

[1]. Vandenberghe S, Mikhaylova E, D'Hoe E, Mollet P, and Karp JS, "Recent developments in time-of-flight PET," EJNMMI Phys., vol. 3, no. 1, 2016. [Online]. Available: 10.1186/s40658-016-0138-3

[2]. Lecoq P, "Pushing the limits in time-of-flight PET imaging," IEEE Trans. Rad. Plas. Med. Sci., vol. 1, no. 6, pp. 473–485, 2017. [Online]. Available: 10.1109/trpms.2017.2756674

[3]. Lecoq P, Morel C, Prior JO et al. , "Roadmap toward the 10 ps time-of-flight PET challenge," Phys. Med. Biol., vol. 65, no. 21, p. 21RM01, 2020. [Online]. Available: 10.1088/1361-6560/ab9500

[4]. Lecoq P, Gonzalez A, Auffray E et al. , "Fast timing in medical imaging," IEEE Trans. Rad. Plas. Med. Sci., 2023. [Online]. Available: 10.1109/trpms.2023.3259464

[5]. Cates JW, Gundacker S, Auffray E, Lecoq P, and Levin CS, "Improved single photon time resolution for analog SiPMs with front end readout that reduces influence of electronic noise," Phys. Med. Biol., vol. 63, no. 18, p. 185022, Sep. 2018. [Online]. Available: 10.1088/1361-6560/aadbcd [PubMed: 30129562]

[6]. Gundacker S, Turtos RM, Auffray E, Paganoni M, and Lecoq P, "High-frequency SiPM readout advances measured coincidence time resolution limits in TOF-PET," Phys. Med. Biol., vol. 64, no. 5, p. 055012, 2019. [Online]. Available: 10.1088/1361-6560/aafd52 [PubMed: 30630146]

[7]. Enoch S, Gola A, Lecoq P, and Rivetti A, "Design considerations for a new generation of SiPMs with unprecedented timing resolution," J. Instrum., vol. 16, no. 02, pp. P02019–P02019, 2021. [Online]. Available: 10.1088/1748-0221/16/02/p02019

[8]. Pratte J-F, Nolet F, Parent S et al. , "3D photon-to-digital converter for radiation instrumentation: Motivation and future works," Sensors, vol. 21, no. 2, p. 598, 2021. [Online]. Available: 10.3390/s21020598 [PubMed: 33467016]

[9]. Cates JW and Choong W-S, "Low power implementation of high frequency SiPM readout for Cherenkov and scintillation detectors in TOF-PET," Phys. Med. Biol., vol. 67, no. 19, p. 195009, 2022. [Online]. Available: 10.1088/1361-6560/ac8963

[10]. Gundacker S, Turtos R, Auffray E, and Lecoq P, "Precise rise and decay time measurements of inorganic scintillators by means of X-ray and 511 keV excitation," Nucl. Instr. Meth. Phys. Res, Sec. A, vol. 891, pp. 42–52, 2018. [Online]. Available: 10.1016/j.nima.2018.02.074

[11]. Wang Z, Dujardin C, Freeman MS et al., "Needs, trends, and advances in scintillators for radiographic imaging and tomography," 2022. [Online]. Available: https://arxiv.org/abs/2212.10322

[12]. Derenzo SE, Choong W-S, and Moses WW, "Fundamental limits of scintillation detector timing precision," Phys. Med. Biol., vol. 59, no. 13, pp. 3261–3286, 2014. [Online]. Available: 10.1088/0031-9155/59/13/3261 [PubMed: 24874216]

[13]. Gundacker S, Turtos RM, Kratochwil N et al. , "Experimental time resolution limits of modern SiPMs and TOF-PET detectors exploring different scintillators and Cherenkov emission," Phys. Med. Biol., vol. 65, no. 2, p. 025001, 2020. [Online]. Available: 10.1088/1361-6560/ab63b4 [PubMed: 31851947]

[14]. Turtos RM, Gundacker S, Auffray E, and Lecoq P, "Towards a metamaterial approach for fast timing in PET: experimental proof-of-concept," Phys. Med. Biol., vol. 64, no. 18, p. 185018, Sep. 2019. [Online]. Available: 10.1088/1361-6560/ab18b3 [PubMed: 30978716]

[15]. Konstantinou G, Lecoq P, Benlloch JM, and Gonzalez AJ, "Metascintillators for ultrafast gamma detectors: A review of current state and future perspectives," IEEE Trans. Rad. Plas. Med. Sci., vol. 6, no. 1, pp. 5–15, 2022. [Online]. Available: 10.1109/trpms.2021.3069624

[16]. Pagano F, Kratochwil N, Salomoni M et al. , "Advances in heterostructured scintillators: toward a new generation of detectors for TOF-PET," Phys. Med. Biol., vol. 67, no. 13, p. 135010, 2022. [Online]. Available: 10.1088/1361-6560/ac72ee

[17]. Gundacker S, Auffray E, Pauwels K, and Lecoq P, "Measurement of intrinsic rise times for various L(Y)SO and LuAG scintillators with a general study of prompt photons to achieve 10 ps in TOF-PET," Phys. Med. Biol., vol. 61, no. 7, pp. 2802–2837, 2016. [Online]. Available: 10.1088/0031-9155/61/7/2802 [PubMed: 26982798]

[18]. Somlai-Schweiger I and Ziegler SI, "CHERENCUBE: Concept definition and implementation challenges of a Cherenkov-based detector block for PET," Med. Phys., vol. 42, no. 4, pp. 1825–1835, 2015. [Online]. Available: 10.1118/1.4914857 [PubMed: 25832073]

[19]. Ariño-Estrada G, Mitchell GS, Kim H et al. , "First Cerenkov charge-induction (CCI) TlBr detector for TOF-PET and proton range verification," Phys. Med. Biol., vol. 64, no. 17, p. 175001, 2019. [Online]. Available: 10.1088/1361-6560/ab35c4 [PubMed: 31344688]

[20]. Ota R, Nakajima K, Ogawa I et al. , "Coincidence time resolution of 30ps FWHM using a pair of Cherenkov-radiator-integrated MCP-PMTs," Phys. Med. Biol., vol. 64, no. 7, p. 07LT01, 2019. [Online]. Available: 10.1088/1361-6560/ab0fce

[21]. Yvon D, Sharyy V, Follin M et al. , "Design study of a scintronic crystal targeting tens of picoseconds time resolution for gamma ray imaging: the ClearMind detector," J. Instrum., vol. 15, no. 07, pp. P07029–P07029, 2020. [Online]. Available: 10.1088/1748-0221/15/07/p07029

[22]. Kratochwil N, Gundacker S, and Auffray E, "A roadmap for sole Cherenkov radiators with SiPMs in TOF-PET," Phys. Med. Biol., vol. 66, no. 19, p. 195001, 2021. [Online]. Available: 10.1088/1361-6560/ac212a

[23]. Kwon SI, Ota R, Berg E et al. , "Ultrafast timing enables reconstruction-free positron emission imaging," Nat. Photon., vol. 15, no. 12, pp. 914–918, 2021. [Online]. Available: 10.1038/s41566-021-00871-2

[24]. Kratochwil N, Gundacker S, Lecoq P, and Auffray E, "Pushing Cherenkov PET with BGO via coincidence time resolution classification and correction," Phys. Med. Biol., vol. 65, no. 11, p. 115004, 2020. [Online]. Available: 10.1088/1361-6560/ab87f9 [PubMed: 32268304]

[25]. Kratochwil N, Auffray E, and Gundacker S, "Exploring Cherenkov emission of BGO for TOF-PET," IEEE Trans. Rad. Plas. Med. Sci., vol. 5, no. 5, pp. 619–629, 2021. [Online]. Available: 10.1109/trpms.2020.3030483

[26]. Efthimiou N, Kratochwil N, Gundacker S et al. , "TOF-PET image reconstruction with multiple timing kernels applied on Cherenkov radiation in BGO," IEEE Trans. Rad. Plas. Med. Sci., vol. 5, no. 5, pp. 703–711, 2021. [Online]. Available: 10.1109/trpms.2020.3048642

[27]. Gonzalez-Montoro A, Pourashraf S, Cates JW, and Levin CS, "Cherenkov radiation–based coincidence time resolution measurements in BGO scintillators," Front. Phys., vol. 10, 2022. [Online]. Available: 10.3389/fphy.2022.816384

[28]. Lecoq P, Korzhik M, and Vasiliev A, "Can transient phenomena help improving time resolution in scintillators?" IEEE Trans. Nucl. Sci., vol. 61, no. 1, pp. 229–234, 2014. [Online]. Available: 10.1109/tns.2013.2282232

[29]. Omelkov SI, Nagirnyi V, Feldbach E et al. , "Intraband luminescence excited in new ways: Low-power X-ray and electron beams," J. Lumin., vol. 191, pp. 61–67, 2017. [Online]. Available: 10.1016/j.jlumin.2017.02.001

[30]. Pots RH, Auffray E, and Gundacker S, "Exploiting cross-luminescence in BaF_2 for ultrafast timing applications using deep-ultraviolet sensitive HPK silicon photomultipliers," Front. Phys., vol. 8, 2020. [Online]. Available: 10.3389/fphy.2020.592875

[31]. Gundacker S, Pots RH, Nepomnyashchikh A et al. , "VUV-SiPMs applied to BaF_2 cross-luminescence detection for high-rate ultrafast timing applications," Phys. Med. Biol., vol. 66, no. 11, p. 114002, 2021. [Online]. Available: 10.1088/1361-6560/abf476

[32]. Ota R and Uenoyama S, "Plasmonic ultraviolet filter for fast-timing applications," Nanophotonics, vol. 12, no. 4, pp. 743–752, 2023. [Online]. Available: 10.1515/nanoph-2022-0704

[33]. Turtos R, Gundacker S, Omelkov S, Auffray E, and Lecoq P, "Light yield of scintillating nanocrystals under X-ray and electron excitation," J. Lumin., vol. 215, p. 116613, nov 2019. [Online]. Available: 10.1016/j.jlumin.2019.116613

[34]. Turtos RM, Gundacker S, Omelkov S et al. , "On the use of CdSe scintillating nanoplatelets as time taggers for high-energy gamma detection," npj 2D Mater. Appl., vol. 3, no. 1, oct 2019. [Online]. Available: 10.1038/s41699-019-0120-8

[35]. Děcká K, Pagano F, Frank I et al. , "Timing performance of lead halide perovskite nanoscintillators embedded in a polystyrene matrix," J. Mater. Chem. C, vol. 10, no. 35, pp. 12836–12843, 2022. [Online]. Available: 10.1039/d2tc02060b

[36]. Be'er O, Gorlach A, Nage A et al., "Free-electron superfluorescence: collective optical dynamics at deep-subwavelength resolution," 2023. [Online]. Available: https://arxiv.org/abs/2301.01608

[37]. Post RF and Schiff LI, "Statistical limitations on the resolving time of a scintillation counter," Phys. Rev., vol. 80, no. 6, pp. 1113–1113, 1950. [Online]. Available: 10.1103/physrev.80.1113

[38]. Fishburn MW and Charbon E, "System tradeoffs in gamma-ray detection utilizing SPAD arrays and scintillators," IEEE Trans. Nucl. Sci., vol. 57, no. 5, pp. 2549–2557, 2010. [Online]. Available: 10.1109/tns.2010.2064788

[39]. Mandai S and Charbon E, "Multi-channel digital SiPMs: Concept, analysis and implementation," in 2012 IEEE Nucl. Sci. Symp. and Med. Imag. Conf. Rec. (NSS/MIC), 2012. [Online]. Available: 10.1109/nssmic.2012.6551429

[40]. Seifert S, van Dam HT, and Schaart DR, "The lower bound on the timing resolution of scintillation detectors," Phys. Med. Biol., vol. 57, no. 7, pp. 1797–1814, 2012. [Online]. Available: 10.1088/0031-9155/57/7/1797 [PubMed: 22410975]

[41]. Vinke R, Olcott PD, Cates JW, and Levin CS, "The lower timing resolution bound for scintillators with non-negligible optical photon transport time in time-of-flight PET," Phys. Med. Biol., vol. 59, no. 20, pp. 6215–6229, 2014. [Online]. Available: 10.1088/0031-9155/59/20/6215 [PubMed: 25255807]

[42]. Venialgo E, Mandai S, Gong T, Schaart DR, and Charbon E, "Time estimation with multichannel digital silicon photomultipliers," Phys. Med. Biol., vol. 60, no. 6, pp. 2435–2452, 2015. [Online]. Available: 10.1088/0031-9155/60/6/2435 [PubMed: 25739661]

[43]. Vinogradov S, "Approximations of coincidence time resolution models of scintillator detectors with leading edge discriminator," Nucl. Instr. Meth. Phys. Res. Sect. A, vol. 912, pp. 149–153, 2018. [Online]. Available: 10.1016/j.nima.2017.11.009

[44]. Therrien AC, Parent S, Tetrault M-A et al. , "Optimization of single photon avalanche diode array detectors with a custom simulator," in 2015 IEEE Nuclear Science Symposium and Medical Imaging Conference (NSS/MIC), 2015. [Online]. Available: 10.1109/nssmic.2015.7581737

[45]. Turtos R, Gundacker S, Polovitsyn A et al. , "Ultrafast emission from colloidal nanocrystals under pulsed X-ray excitation," J. Instrum., vol. 11, no. 10, pp. P10015–P10015, 2016. [Online]. Available: 10.1088/1748-0221/11/10/p10015

[46]. Tetrault M-A, Therrien AC, Lemaire W, Fontaine R, and Pratte J-F, "TDC array tradeoffs in current and upcoming digital SiPM detectors for time-of-flight PET," IEEE Trans. Nucl. Sci., vol. 64, no. 3, pp. 925–932, 2017. [Online]. Available: 10.1109/tns.2017.2665878

[47]. Cates JW and Levin CS, "Evaluation of a clinical TOF-PET detector design that achieves ⩽100 ps coincidence time resolution," Phys. Med. Biol., vol. 63, no. 11, p. 115011, 2018. [Online]. Available: 10.1088/1361-6560/aac504 [PubMed: 29762136]

[48]. Toussaint M, Loignon-Houle F, Dussault J-P, and Lecomte R, "Analytical model of DOI-induced time bias in ultra-fast scintillation detectors for TOF-PET," Phys. Med. Biol., vol. 64, no. 6, p. 065009, 2019. [Online]. Available: 10.1088/1361-6560/ab038b [PubMed: 30703756]

[49]. Loignon-Houle F, Toussaint M, Lee MS, Cates JW, and Lecomte R, "Experimental validation of a coincidence time resolution metric including depth-of-interaction bias for TOF-PET," Phys. Med. Biol., vol. 65, no. 24, p. 245004, 2020. [Online]. Available: 10.1088/1361-6560/aba7d0 [PubMed: 32693396]

[50]. Loignon-Houle F, Gundacker S, Toussaint M et al. , "DOI estimation through signal arrival time distribution: a theoretical description including proof of concept measurements," Phys. Med. Biol., vol. 66, no. 9, p. 095015, 2021. [Online]. Available: 10.1088/1361-6560/abf604

[51]. Roncali E, Kwon SI, Jan S, Berg E, and Cherry SR, "Cerenkov light transport in scintillation crystals explained: realistic simulation with GATE," Biomed. Phys. Eng. Express, vol. 5, no. 3, p. 035033, 2019. [Online]. Available: 10.1088/2057-1976/ab0f93 [PubMed: 33304614]

[52]. Schaart DR, "Physics and technology of time-of-flight PET detectors," Phys. Med. Biol., vol. 66, no. 9, p. 09TR01, 2021. [Online]. Available: 10.1088/1361-6560/abee56

[53]. Gundacker S, Auffray E, Jarron P, Meyer T, and Lecoq P, "On the comparison of analog and digital SiPM readout in terms of expected timing performance," Nucl. Instr. Meth. Phys. Res, Sec. A, vol. 787, pp. 6–11, 2015. [Online]. Available: 10.1016/j.nima.2014.10.020

[54]. Děcká K, Kr J´ al, F. Hájek et al. , “Scintillation response enhancement in nanocrystalline lead halide perovskite thin films on scintillating wafers,” Nanomaterials, vol. 12, no. 1, p. 14, 2021. [Online]. Available: 10.3390/nano12010014 [PubMed: 35009964]

[55]. Jan S, Santin G, Strul D et al. , “GATE: a simulation toolkit for PET and SPECT,” Phys. Med. Biol., vol. 49, no. 19, pp. 4543–4561, 2004. [Online]. Available: 10.1088/0031-9155/49/19/007 [PubMed: 15552416]

[56]. Stockhoff M, Jan S, Dubois A, Cherry SR, and Roncali E, “Advanced optical simulation of scintillation detectors in GATE V8.0: first implementation of a reflectance model based on measured data,” Phys. Med. Biol., vol. 62, no. 12, pp. L1–L8, 2017. [Online]. Available: 10.1088/1361-6560/aa7007 [PubMed: 28452339]

[57]. Trigila C, private communication, Nov. 2021.

[58]. Gundacker S, Auffray E, Frisch B et al. , “Time of flight positron emission tomography towards 100 ps resolution with L(Y)SO: an experimental and theoretical analysis,” J. Instrum., vol. 8, no. 07, pp. P07014–P07014, 2013. [Online]. Available: 10.1088/1748-0221/8/07/p07014

[59]. Clinthorne N, Petrick N, Rogers W, and Hero A, “A fundamental limit on timing performance with scintillation detectors,” IEEE Trans. Nucl. Sci., vol. 37, no. 2, pp. 658–663, apr 1990. [Online]. Available: 10.1109/23.106694

[60]. Clinthorne NH, Hero AO, Petrick NA, and Rogers WL, “Lower bounds on scintillation detector timing performance,” Nucl. Instr. Meth. Phys. Res. Sect. A, vol. 299, no. 1–3, pp. 157–161, Dec. 1990. [Online]. Available: 10.1016/0168-9002(90)90767-z

[61]. Lucchini M, Chung W, Eno S et al. , “New perspectives on segmented crystal calorimeters for future colliders,” J. Instrum., vol. 15, no. 11, pp. P11005–P11005, 2020. [Online]. Available: 10.1088/1748-0221/15/11/p11005

[62]. Gorman J and Hero A, “Lower bounds for parametric estimation with constraints,” IEEE Trans. Inf. Theory, vol. 36, no. 6, pp. 1285–1301, 1990. [Online]. Available: 10.1109/18.59929

[63]. Acerbi F and Gundacker S, “Understanding and simulating SiPMs,” Nucl. Instr. Meth. Phys. Res. Sect. A, vol. 926, pp. 16–35, 2019. [Online]. Available: 10.1016/j.nima.2018.11.118

[64]. Cates JW, Vinke R, and Levin CS, “Analytical calculation of the lower bound on timing resolution for PET scintillation detectors comprising high-aspect-ratio crystal elements,” Phys. Med. Biol., vol. 60, no. 13, pp. 5141–5161, 2015. [Online]. Available: 10.1088/0031-9155/60/13/5141 [PubMed: 26083559]

[65]. Gola A, Acerbi F, Capasso M et al. , “NUV-sensitive silicon photomultiplier technologies developed at Fondazione Bruno Kessler,” Sensors, vol. 19, no. 2, p. 308, 2019. [Online]. Available: 10.3390/s19020308 [PubMed: 30646553]

[66]. Lecoq P and Gundacker S, “SiPM applications in positron emission tomography: toward ultimate PET time-of-flight resolution,” Eur. Phys. J. Plus, vol. 136, no. 3, 2021. [Online]. Available: 10.1140/epjp/s13360-021-01183-8

[67]. Roques-Carmes C, Kooi SE, Yang Y et al. , “Free-electron–light interactions in nanophotonics,” Appl. Phys. Rev., vol. 10, no. 1, p. 011303, 2023. [Online]. Available: 10.1063/5.0118096

[68]. Loignon-Houle F, Charlebois SA, Fontaine R, and Lecomte R, “Monte Carlo simulations of energy, time and spatial evolution of primary electrons generated by 511 keV photons in various scintillators,” Nucl. Instr. Meth. Phys. Res. Sect. A, vol. 1030, p. 166449, 2022. [Online]. Available: 10.1016/j.nima.2022.166449

[69]. Kurman Y, Shultzman A, Segal O, Pick A, and Kaminer I, “Photonic-crystal scintillators: Molding the flow of light to enhance X-ray and γ-ray detection,” Phys. Rev. Lett., vol. 125, no. 4, 2020. [Online]. Available: 10.1103/physrevlett.125.040801

[70]. Kurman Y, Lahav N, Schuetz R et al., “Purcell-enhanced X-ray scintillation,” 2023. [Online]. Available: https://arxiv.org/abs/2302.01300

[71]. Shultzman A, Segal O, Kurman Y, Roques-Carmes C, and Kaminer I, “Enhanced imaging using inverse design of nanophotonic scintillators,” Adv. Opt. Mater., p. 2202318, 2023. [Online]. Available: 10.1002/adom.202202318

[72]. Kaminer I, Katan YT, Buljan H et al. , “Efficient plasmonic emission by the quantum Cerenkov effect from hot carriers in graphene,” Nature Commun., vol. 7, no. 1, 2016. [Online]. Available: 10.1038/ncomms11880

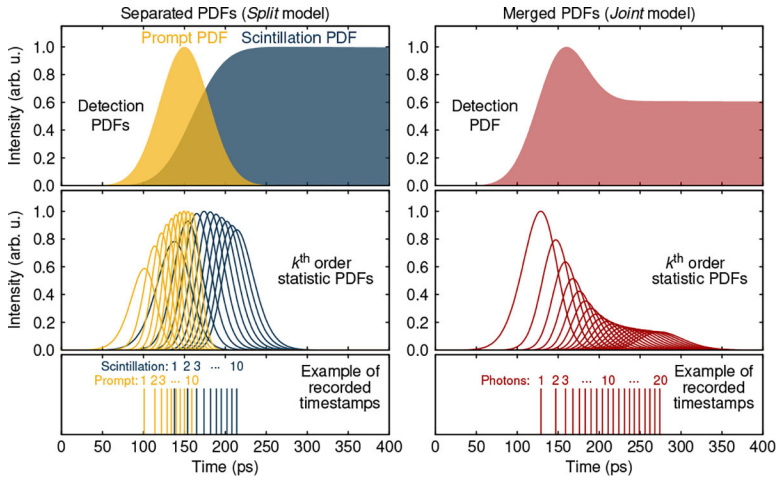

Fig. 1.

Detection PDF(s) (top), order statistics PDFs (middle) and examples of a set of recorded timestamps (bottom) for the two models where the prompt and scintillation detection PDFs are either separated (left) or merged (right) together (Dirac prompt emission, scintillation with rise and decay time of 10 ps and 30 ns, SPTR of 30 ps rms). Order statistics PDFs of the first detected photons (15 prompt and 5000 scintillation photons in total) are displayed either for the first 10 photons of each regime (left) or the first 20 photons without knowledge of the photon regime (right).

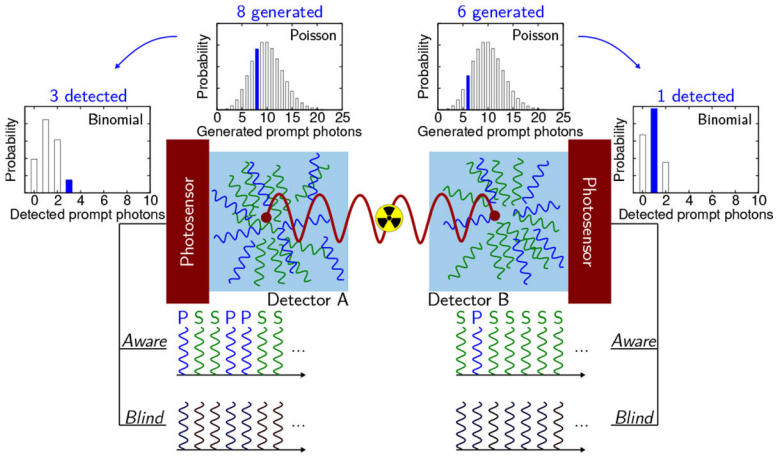

Fig. 2.

Example of the scintillation (green waves) and prompt (blue waves) photons fluctuations on their production and detection. Being *aware* or *blind* to the nature of the detected photons provides a different insight on the observed timestamps.

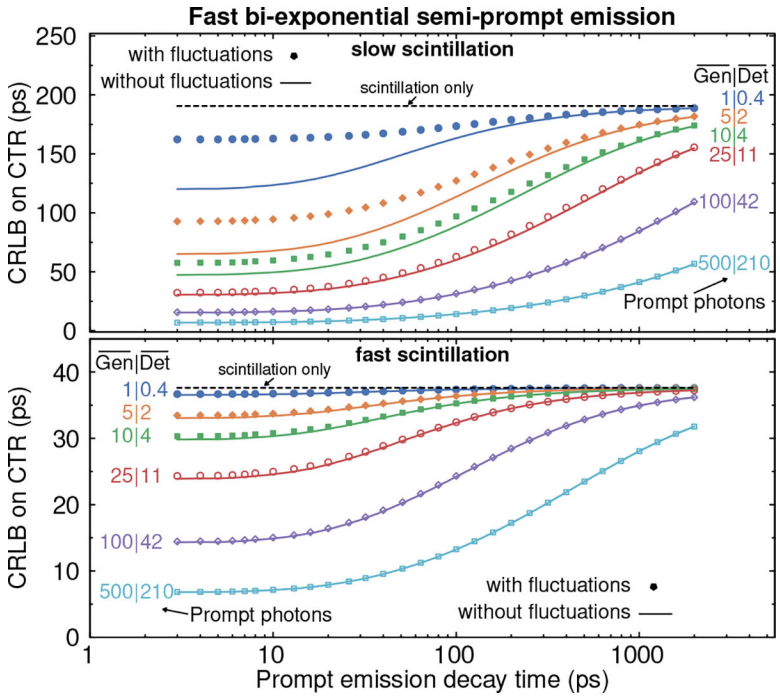

Fig. 3.

CRLB on CTR ($2.355 \times \sigma_{coinc}$) as a function of the prompt emission decay time for six values of prompt photon yield (mean generated and mean detected values are shown) with (symbols) or without (lines) fluctuations, calculated with the *Split* model. The scintillation population is assumed having similar properties as a BGO crystal (top plot, rise time of 8ps, decay time of 46/365 ns(8%/92%), light yield of 10 700 phMeV^{-1}) or a LSO:Ce:0.2% Ca crystal (bottom plot, rise time of 9ps, decay time of 10.8/35 ns (5%/95%), light yield of 39 200 phMeV^{-1} with emission properties from [13]. The LTE and PDE were set as 70% and 60%. A photodetection Gaussian response with 30 ps rms SPTR was defined. The dotted lines indicate the CTR when only scintillation is produced.

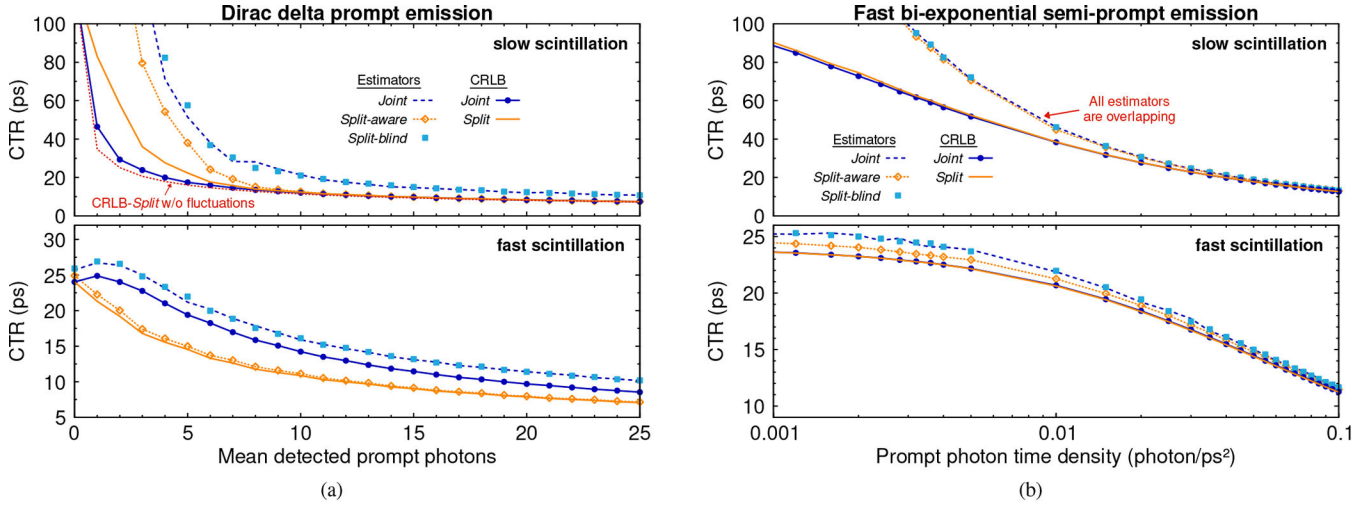

Fig. 4.

CTR of estimators (*aware* and *blind*) and CRLB on CTR (a) as a function of the mean number of detected prompt photons for a Dirac delta emission and (b) as a function of the prompt photon time density for a fast bi-exponential semi-prompt emission (rise and decay times of 10 ps and 500ps, respectively). The prompt and semi-prompt photons were accompanied either with slow scintillation (top) or fast scintillation (bottom) with properties defined in the caption of Fig. 3. CTR values were obtained either with the *Joint* or the *Split* model and the SPTR was set at 10 ps rms.

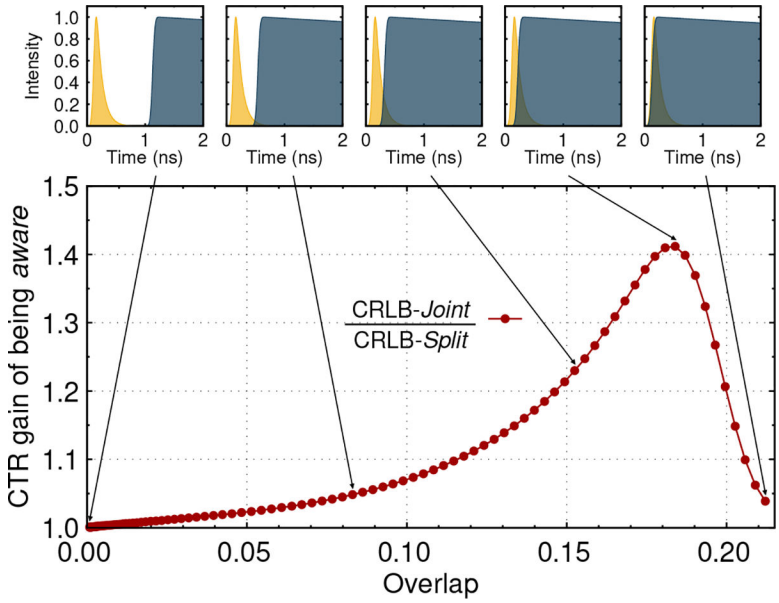

Fig. 5.

Ratio between CRLB-*Joint* and CRLB-*Split* for a bi-exponential semi-prompt emission (rise and decay time of 1 ps and 100 ps, 10 detected prompt photons) and a LSO:Ce:0.2%Ca scintillation emission shifted in time to create different levels of overlap (SPTR of 30 ps rms). The overlap between the PDFs was calculated with $\int_0^\infty \min(p_P(t), p_S(t))\mathrm{d}t$. Varying the scintillation rise time to change the overlap yielded similar outcome.

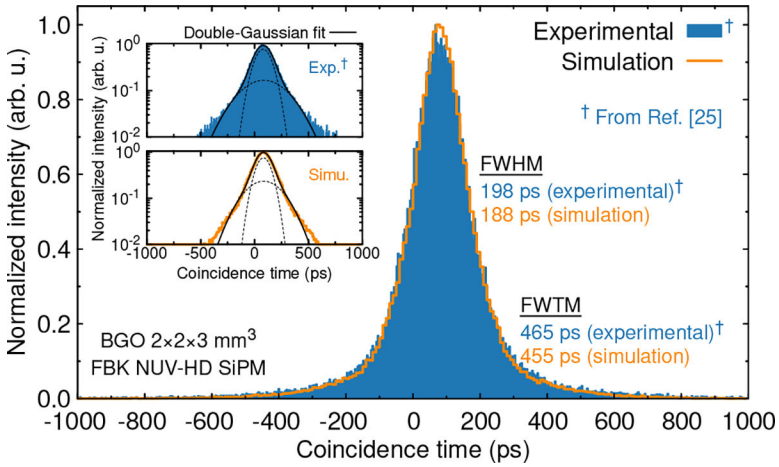

Fig. 6.

Coincidence time distribution of simulated data obtained from the *Split* model and experimental data given in [25], both for a 2×2×3 mm^3 BGO coupled to a FBK NUV-HD SiPM. The inset plot shows the same data with a logarithmic scale and the double-Gaussian fits used to extract the FWHM and FWTM values.

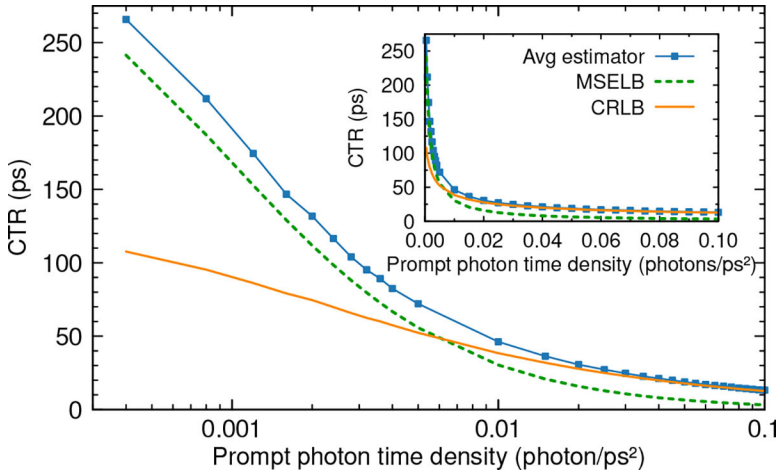

Fig. 7.

CTR as a function of the prompt photon time density for the MSE lower bound of Eq. (13), the average (Avg) *blind* estimator and the CRLB of the *Split* model. The inset plot shows the same results on a linear scale for the photon time density. The signal was defined as the scintillation from BGO and a semi-prompt population (SPTR of 10 ps rms in the *Split* model PDFs).